The LC3 recruitment mechanism is separate from Atg9L1-dependent membrane formation in the autophagic response against *Salmonella*

Shun Kageyama[a], Hiroko Omori[b], Tatsuya Saitoh[c], Takefumi Sone[d], Jun-Lin Guan[e], Shizuo Akira[c], Fumio Imamoto[d], Takeshi Noda[a,f], and Tamotsu Yoshimori[a,f]

[a]Laboratory of Intracellular Membrane Dynamics, Graduate School of Frontier Biosciences, Osaka University, 3-1 Yamadaoka, Suita, Osaka 565-0871, Japan; [b]Research Institute for Microbial Diseases, Osaka University, 3-1 Yamadaoka, Suita, Osaka 565-0871, Japan; [c]Laboratory of Host Defense, WPI Immunology Frontier Research Center (IFReC), and Department of Host Defense, Research Institute for Microbial Diseases, Osaka University 3-1 Yamadaoka, Suita, Osaka 565-0871, Japan; [d]Department of Molecular Biology, Research Institute for Microbial Diseases, Osaka University, 3-1 Yamadaoka, Suita, Osaka 565-0871, Japan; [e]Department of Internal Medicine–MMG, University of Michigan Medical School, Ann Arbor, MI 48109; [f]Department of Genetics, Graduate School of Medicine, Osaka University, 2-2 Yamadaoka, Suita, Osaka 565-0871, Japan

ABSTRACT ***Salmonella*** **develops into resident bacteria in epithelial cells, and the autophagic machinery (Atg) is thought to play an important role in this process. In this paper, we show that an autophagosome-like double-membrane structure surrounds the *Salmonella* still residing within the *Salmonella*-containing vacuole (SCV). This double membrane is defective in Atg9L1- and FAK family-interacting protein of 200 kDa (FIP200)-deficient cells. Atg9L1 and FIP200 are important for autophagy-specific recruitment of the phosphatidylinositol 3-kinase (PI3K) complex. However, in the absence of Atg9L1, FIP200, and the PI3K complex, LC3 and its E3-like enzyme, the Atg16L complex, are still recruited to *Salmonella*. We propose that the LC3 system is recruited through a mechanism that is independent of isolation membrane generation.**

Monitoring Editor
Akihiko Nakano
RIKEN

Received: Nov 12, 2010
Revised: Apr 14, 2011
Accepted: Apr 21, 2011

INTRODUCTION

Salmonella enterica serovar Typhimurium (*S. typhimurium*) is a Gram-negative bacterial pathogen that causes food poisoning and gastroenteritis in humans (Finlay and Brumell, 2000; Haraga *et al.*, 2008). *Salmonella* infects small intestinal epithelial cells and develops as a resident bacterium in this niche, which allows this bacterium to cause widespread infection. Therefore understanding the mechanisms that *Salmonella* uses to develop into a resident bacterium in host cells is important in controlling *Salmonella* infection. *Salmonella* can invade epithelial cells by forming a specialized single-membrane organelle, termed the *Salmonella*-containing vacuole (SCV), using a type III secretion system (TTSS), which is a needle-like structure that injects effector proteins into the host cell cytosol (Hueck, 1998; Finlay and Brumell, 2000). In the early phase following invasion, SCVs temporarily acquire early endosome markers, such as Rab5, transferrin receptor, and EEA1; late endosomal proteins, such as LAMP1, are then substituted for these proteins (Bakowski *et al.*, 2008; Drecktrah *et al.*, 2008; Huang and Brumell, 2009). A few hours postinfection, *Salmonella* rearranges the SCVs into long tubular structures called *Salmonella*-induced filaments (Sifs), where the bacteria stably propagate (Bakowski *et al.*, 2008; Drecktrah *et al.*, 2008; Huang and Brumell, 2009).

It was previously reported that a portion of invading *S. typhimurium* is associated with LC3, a typical marker of autophagy, which is an intracellular bulk protein degradation system (Kabeya *et al.*, 2000; Birmingham *et al.*, 2006). The intracellular replication of

This article was published online ahead of print in MBoC in Press (http://www.molbiolcell.org/cgi/doi/10.1091/mbc.E10-11-0893) on April 27, 2011.

Address correspondence to: Takeshi Noda (takenoda@fbs.osaka-u.ac.jp); Tamotsu Yoshimori (tamyoshi@fbs.osaka-u.ac.jp).

Abbreviations used: BSA, bovine serum albumin; CLEM, correlative light microscopy–electron microscopy; DMSO, dimethyl sulfoxide; EM, electron microscopy; EYFP, enhanced yellow fluorescent protein; FBS, fetal bovine serum; FIP200, FAK family-interacting protein of 200 kDa; FNBP1L, formin-binding protein 1-like; GFP, green fluorescent protein; KO MEF, knockout mouse embryonic fibroblast; LB, lysogeny broth; MOI, multiplicity of infection; NA, numerical aperture; PBS, phosphate-buffered saline; PI3K, phosphatidylinositol 3-kinase; PI3P, phosphatidylinositol 3-phosphate; *S. typhimurium*, *Salmonella enterica* serovar Typhimurium; SCV, *Salmonella*-containing vacuole; SECFP, superenhanced cyan fluorescent protein; Sifs, *Salmonella*-induced filaments; TTSS, type III secretion system; ULK, uncoordinated 51-like kinase; WIPI, WD-repeat protein interacting with phosphoinositides.

S. typhimurium is increased in autophagy-defective host cells compared with wild-type cells (Birmingham *et al.*, 2006; Sun *et al.*, 2008; Fujita *et al.*, 2009), and ultimately leads to host cell death. Therefore autophagy protects host cells from pathogenic bacteria. On the other hand, it is possible that the autophagic machinery plays a role in establishing resident bacteria. These processes are collectively called *xenophagy*, and the molecular mechanisms that govern these processes are just now beginning to be analyzed (Levine, 2005; Deretic and Levine, 2009; Huang and Brumell, 2009; Noda and Yoshimori, 2009). Macroautophagy is a nonselective bulk degradation system; however, *S. typhimurium* appears to be selectively isolated in xenophagy. Therefore analyzing xenophagy will provide additional information on how the machinery of autophagy functions. The autophagy machinery is generally composed of Atg proteins that are highly conserved from yeast to mammals (Yoshimori and Noda, 2008; Nakatogawa *et al.*, 2009). Therefore we decided to analyze how Atg proteins function in *S. typhimurium* xenophagy. In this paper, we show that Atg proteins are recruited near *S. typhimurium*, and we provide new insight into their functions during this process. Atg9L1 is absolutely required for the formation of an autophagosome-like double membrane around the SCV. Furthermore, LC3 systems are recruited to proximity to *Salmonella*, even in the absence of autophagosome-like structures in Atg9L1 knockout mouse embryonic fibroblasts (KO MEFs). These results indicate the existence of a recruitment mechanism of the LC3 system independent of isolation membrane generation.

RESULTS

LC3 associates with *S. typhimurium* through an LC3-lipidation reaction

It was previously reported that a population of *S. typhimurium* in infected mammalian epithelial cells was surrounded by green fluorescent protein (GFP)-LC3 (Birmingham *et al.*, 2006). To examine the detailed process by which GFP-LC3 associates with *S. typhimurium*, we performed time-lapse imaging of live cells. MEFs stably expressing GFP-LC3 were infected with *S. typhimurium* expressing the fluorescent protein mCherry. Single (Figure 1Aa and Supplemental Movie S1) or multiple (Figure 1Ab and Movie S2) GFP-LC3 puncta appeared in close contact with *S. typhimurium*, and the GFP-LC3 signal then elongated laterally, along with the bacteria, and finally completely surrounded the bacteria. We speculate that the multi-puncta pattern represents a focus located on the posterior surface of *S. typhimurium* that elongated with several finger-like edges, which appear as distinct puncta. The other pattern was also observed in some instances (~23%; Figure 1Ac and Movie S3). These observations clearly established that LC3 actively associates with *S. typhimurium*.

We next examined the molecular mechanism of LC3 association. LC3 is a ubiquitin-like protein that undergoes phosphatidylethanolamine modifications at its C-terminus through a reaction that is catalyzed by the E1 (Atg7), E2 (Atg3), and E3 (Atg16L1 complex consisting of Atg12, Atg5, and Atg16L1) enzymes (Ichimura *et al.*, 2000; Kabeya *et al.*, 2000; Mizushima *et al.*, 2001; Fujita *et al.*, 2008b). In macroautophagy, LC3 recruitment is defective in KO MEFs lacking these genes (*ATG7*, *ATG3*, and *ATG5*) (Mizushima *et al.*, 2001; Kuma *et al.*, 2004; Komatsu *et al.*, 2006; Sou *et al.*, 2008). Similarly, we found that GFP-LC3 recruitment during *S. typhimurium* infection was totally defective in Atg7, Atg3, and Atg5 KO cells (Figure 1, B and C). These results indicate that the dynamic recruitment of LC3 to *S. typhimurium* requires the LC3-lipidation reaction.

Previously, it was reported that *S. typhimurium* growth was highly accelerated in Atg5 KO cells compared to wild-type cells (Birmingham *et al.*, 2006). We investigated the growth of intracellular bacteria in a series of Atg KO cells. The infection efficiency of *S. typhimurium* was similar in wild-type and Atg KO cells (Supplemental Figure S1). In addition, we used an inactive Atg4B mutant, Atg4B^{C74A}, which is a protease that processes LC3s and its paralogues, such as GABARAP and GATE-16. Expression of the Atg4B^{C74A} mutant resulted in the sequestration of LC3 in a stable complex with the Atg4B^{C74A} mutant, and thus inhibited LC3 recruitment to the autophagosome (Fujita *et al.*, 2008a). As shown in Figure 1, D–I, *S. typhimurium* grew more efficiently in Atg7, Atg3, and Atg5 KO cells and Atg4B^{C74A}-expressing cells than in wild-type cells (Figure 1, D–F and I, and Figure S1, A–F). These results indicate that LC3s must be recruited to *S. typhimurium* to suppress the growth of this bacterium.

Atg9L1 is dispensable for LC3 recruitment but indispensable for *S. typhimurium* growth suppression

Atg9 is a membrane-spanning protein that is essential for autophagosome formation in macroautophagy (Noda *et al.*, 2000; Yamada *et al.*, 2005; Young *et al.*, 2006; Saitoh *et al.*, 2009). We next examined the role of Atg9L1 in *Salmonella* xenophagy by monitoring the localization of GFP-LC3. GFP-LC3 efficiently associated with *S. typhimurium* in Atg9L1 KO cells (Figure 1, B and C), indicating that LC3 can be recruited to *S. typhimurium* through an Atg9L1-independent mechanism. Therefore we asked whether Atg9L1 plays a role in suppressing *S. typhimurium* growth by performing a colony-forming assay. Interestingly, bacterial growth was not suppressed in Atg9L1 KO cells. These results suggest that LC3 recruitment to *S. typhimurium* is not sufficient to suppress intracellular bacterial growth (Figure 1G).

These results prompted us to investigate how LC3 recruitment is related to *S. typhimurium* growth in Atg9L1 KO cells. We examined the fate of a single *S. typhimurium* cell from 1 to 6 h postinfection by time-lapse imaging. Wild-type or Atg9L1 KO cells stably expressing GFP-LC3 were infected with *S. typhimurium* expressing mCherry and incubated for 1 h. Then a GFP-LC3–positive *S. typhimurium* was recorded for 5 h with time-lapse imaging at 4-min intervals. In wild-type cells, more than 70% of the GFP-LC3–positive *S. typhimurium* cells did not grow to more than 5 cells after 6 h, and only a small population grew to >10 cells (Figure 2, A and B, and Movie S4). On the other hand, in Atg9L1 KO cells, almost 60% of the GFP-LC3–positive *S. typhimurium* grew to >10 cells after 6 h (Figure 2, A and B, and Movie S5). The growth of GFP-LC3–negative *S. typhimurium* was similar between wild-type and Atg9L1 KO cells (Figure S2, A and B, and Movies S6 and S7). Significantly, the GFP-LC3 signal was diminished at a relatively early phase in wild-type cells (Figure 2C and Movie S4). However, the GFP-LC3 signal surrounding the bacteria was retained until late in infection in Atg9L1 KO cells (Figure 2, A [4–5 h postinfection] and C, and Movie S5). These results clearly indicate that GFP-LC3–positive membranes in Atg9L1 KO cells lack the ability to suppress *S. typhimurium* proliferation.

Atg9L1-positive puncta surround *S. typhimurium* prior to the appearance of LC3

To gain further insight into how Atg9L1 is involved in these processes, we next performed time-lapse live-cell imaging of Atg9L1-GFP during bacterial infection. MEFs stably expressing Atg9L1-GFP were infected with *S. typhimurium* expressing mCherry. In addition to localizing to the Golgi, as previously reported (Young *et al.*, 2006), numerous Atg9L1-GFP–positive puncta moved within the cytosol irrespective of *S. typhimurium* infection (Figure 3A [arrows and

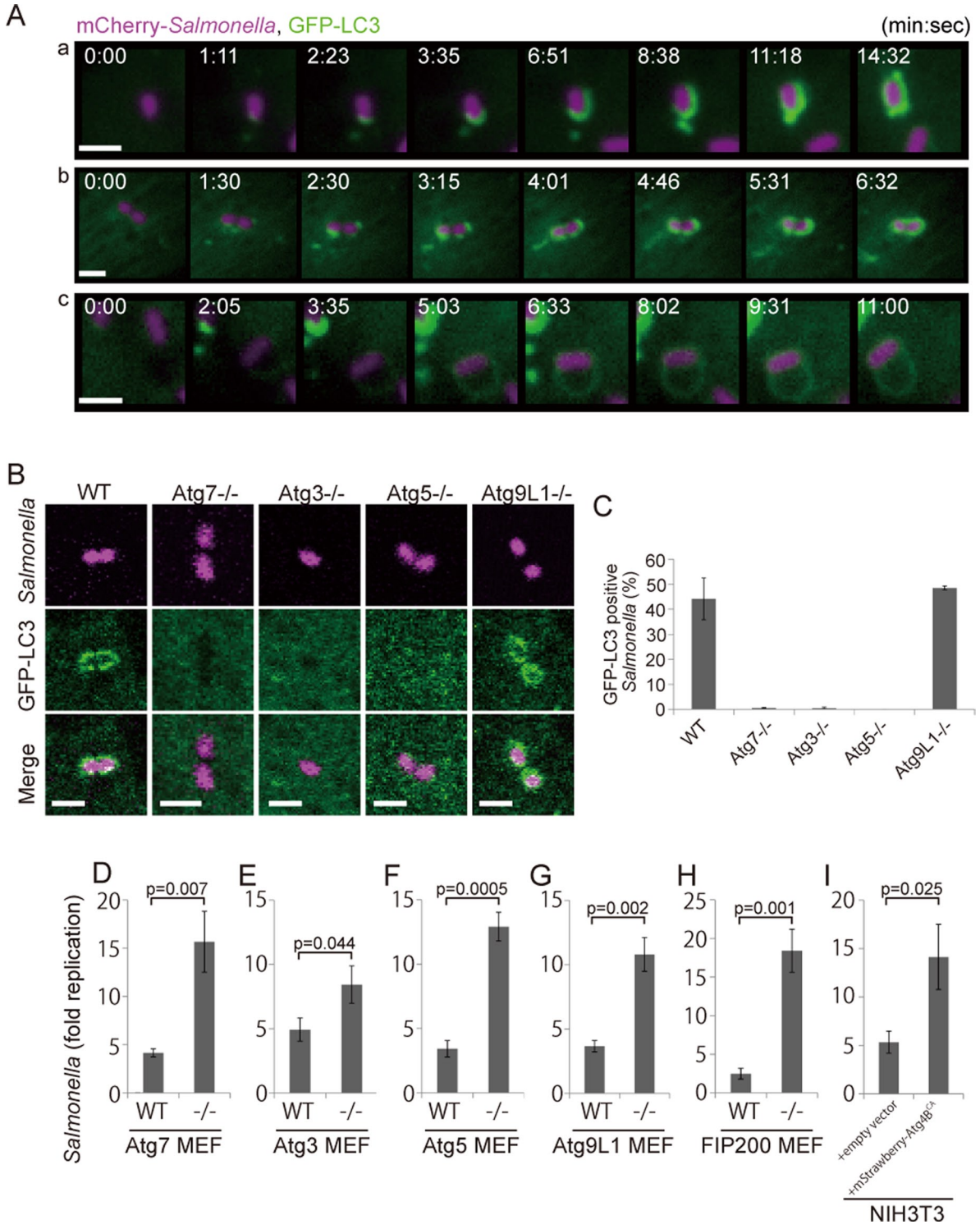

FIGURE 1: GFP-LC3 association with infected *S. typhimurium*. (A) MEFs stably expressing GFP-LC3 were infected with *S. typhimurium* expressing mCherry for 5 min and then washed to remove the inoculum. The cells were imaged at ~15-s intervals using a fluorescence inverted microscope. Live-cell imaging is shown and the elapsed time after the association of GFP-LC3 is indicated. Scale bar: 1 μm. (B and C) MEFs with deletions in each of the noted Atg genes and their parental cells stably expressing GFP-LC3 were infected with *S. typhimurium* expressing mCherry for 1 h at an MOI of 10 and then washed. The samples were fixed, and the GFP-LC3 association rate was examined by fluorescence microscopy. The average ± SD is shown for three independent experiments where at least 100 bacteria were counted. Scale bar: 2 μm. (D–I) MEFs of the noted Atg KOs and their parental cells or NIH3T3 cells with or without Atg4B^{C74A} expression were infected with *S. typhimurium* for 10 min in DMEM without antibiotics at an MOI of 100. After infection, the cells were washed to remove extracellular *S. typhimurium* and incubated in DMEM containing gentamicin for 6 h. The cell lysates were plated on LB plates and the number of colonies was counted after a 1-d incubation at 37°C. The average ± SD of three independent experiments is shown.

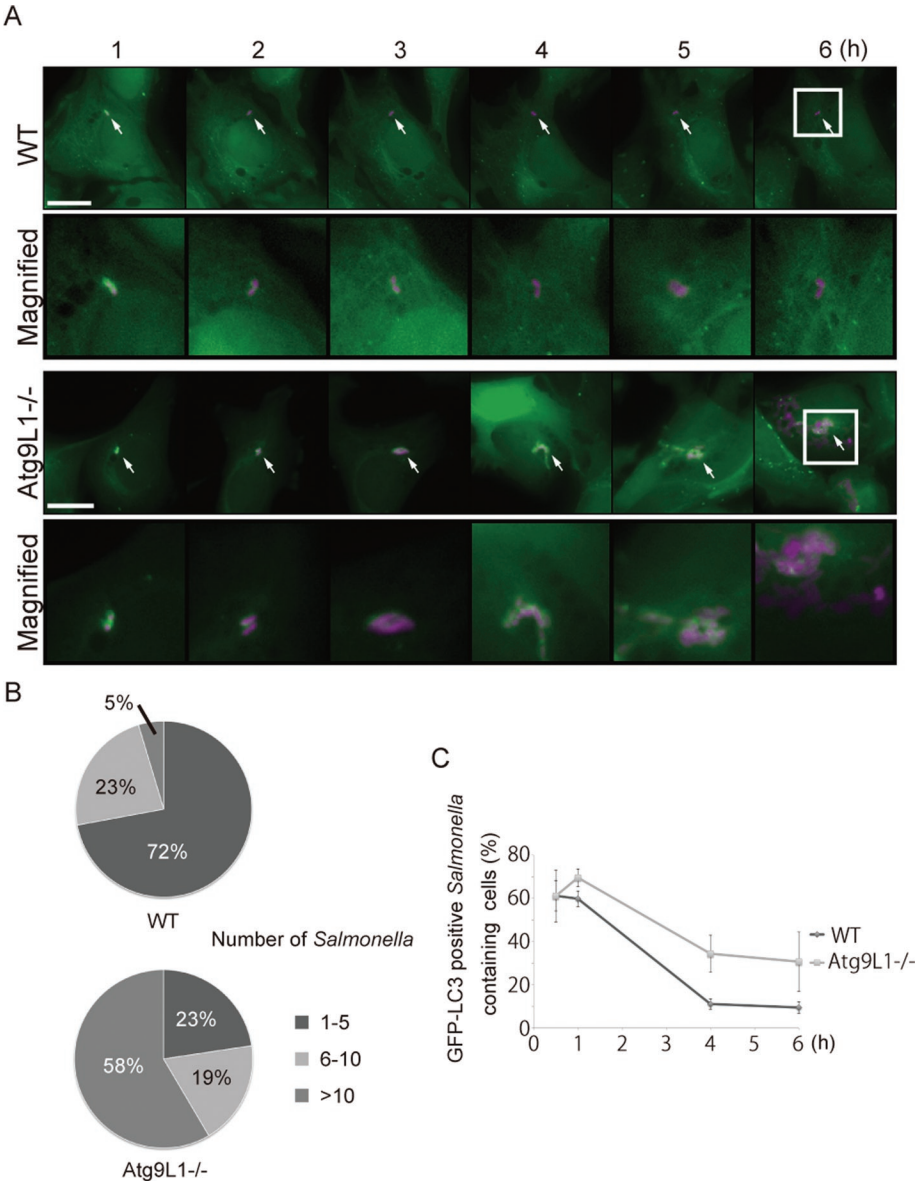

FIGURE 2: Extended trace of GFP-LC3 association with *Salmonella*. (A) Wild-type or Atg9L1 KO MEFs stably expressing GFP-LC3 were infected with *S. typhimurium* expressing mCherry for 5 min at an MOI of 100, washed, and then incubated for 1 h. One GFP-LC3–positive *S. typhimurium* was followed by time-lapse imaging at 4-min intervals with the automated trace system of MetaMorph until 6 h postinfection. The elapsed time is indicated. Scale bar: 20 μm. (B) The final number of *S. typhimurium* in each cell was determined after 6 h of time-lapse imaging and grouped as indicated. (C) Cells stably expressing GFP-LC3 were infected with *S. typhimurium* expressing mCherry and incubated. The cells were fixed at the indicated time points and examined by fluorescence microscopy. At least 100 cells were counted for each experiment. The average ± SD is shown for three independent experiments.

arrowheads], and Movie S8). Using immunofluorescence, we determined that at least some of these puncta colocalized with EEA1, an early endosomal marker (Figure 3B). There were several intense punctate signals that gradually associated with *S. typhimurium*, and these signals moved dynamically (Figure 3C [arrowheads] and Movie S9). Furthermore, over a longer time period, the Atg9L1-GFP signals gradually surrounded *S. typhimurium*, and after a certain period of time (10–60 min), the signal disappeared from the area containing *S. typhimurium* (Figure 3C and Movie S9). To relate these findings with the localization of LC3, we next generated cells stably expressing Atg9L1 tagged with superenhanced cyan fluorescent protein (SECFP)- and enhanced yellow fluorescent protein (EYFP)-LC3, and performed time-lapse live-cell imaging. Atg9L1-SECFP signals surrounding *S. typhimurium* become apparent before LC3 was recruited to the bacteria (Figure 3D [2 min, 3 s]). Next the EYFP-LC3 signals appeared and colocalized with Atg9L1-SECFP (Figure 3D [4 min, 38 s]). Finally, the Atg9L1-SECFP signals disappeared from *S. typhimurium* even when the EYFP-LC3 signals remained (Figure 3D [9 min, 16 s] and Movie S10). Swapping the SECFP and EYFP tags did not change the results (Figure S3 and Movie S11). These results raised the possibility that Atg9 plays a role during *S. typhimurium* infection that is independent of the function of LC3.

We examined the recruitment of other Atg proteins to *S. typhimurium* to determine if it is affected in Atg9L1 KO cells. We previously reported that the membrane localization of the Atg16L1 complex (E3) determines the site where LC3 lipidation occurs (Fujita *et al.*, 2008b). Consistent with LC3 recruitment, GFP-Atg5, a subunit of the Atg16L1 complex, was also recruited near *S. typhimurium* in Atg9L1 KO cells as well as wild-type cells (Figure 4A). Therefore the Atg16L1 complex is specifically recruited to *S. typhimurium* independently of Atg9L1.

Phosphatidylinositol 3-kinase is not necessary for LC3 recruitment during *S. typhimurium* infection

Atg14L is a specific subunit of the class III phosphatidylinositol 3-kinase (PI3K) complex (Vps34) involved in macroautophagy (Itakura *et al.*, 2008; Sun *et al.*, 2008; Matsunaga *et al.*, 2009, 2010; Zhong *et al.*, 2009). WD-repeat protein interacting with phosphoinositides (WIPI)-1 is a homologue of the essential yeast autophagy protein, Atg18, and binds to phosphatidylinositol 3-phosphate (PI3P) (Proikas-Cezanne *et al.*, 2004). They localize to the autophagosomes as the autophagosomes form (Proikas-Cezanne *et al.*, 2004; Itakura *et al.*, 2008; Matsunaga *et al.*, 2009). As shown in Figure 4, B and C, Atg14L and WIPI-1 were also recruited to *S. typhimurium* in wild-type cells. This result indicated the autophagy-specific PI3K complex might also be involved in *Salmonella* xenophagy. Interestingly, these localizations were defective in Atg9L1 KO cells (Figure 4, B and C).

Because Atg14L and WIPI-1 localization was not observed in Atg9L1 KO cells, we investigated whether PI3K helps recruit LC3 to *S. typhimurium*. During macroautophagy, LC3 recruitment is abolished by treating with wortmannin, a potent PI3K inhibitor (Kabeya *et al.*, 2000). Cells stably expressing GFP-LC3 were treated with wortmannin 15 min prior to *S. typhimurium* infection, and then the number of *S. typhimurium*-infected cells was determined 60 min postinfection. As shown in Figure 5A, wortmannin treatment

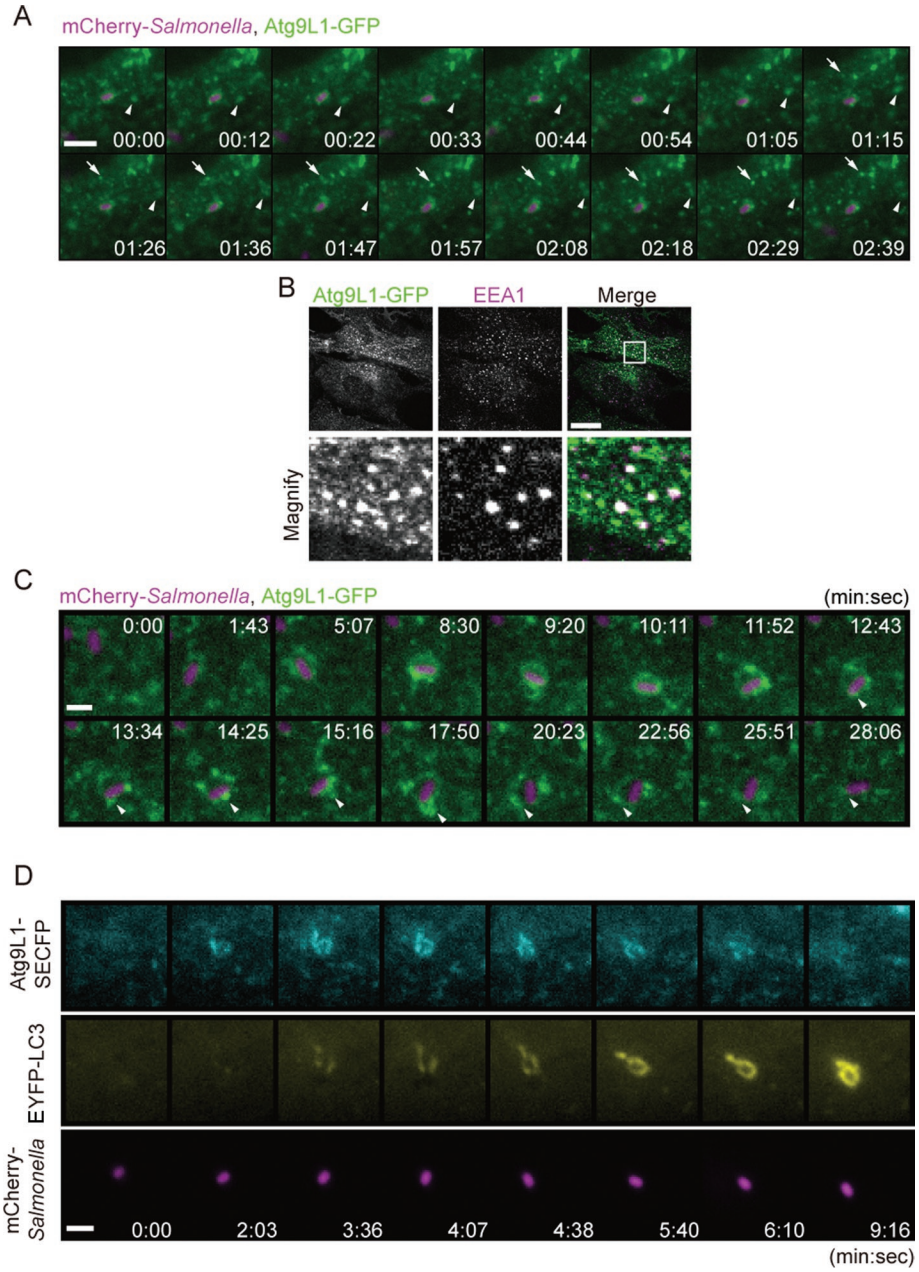

FIGURE 3: Live-cell imaging of Atg9L1 localization. (A and C) MEFs stably expressing Atg9L1-GFP were infected with *S. typhimurium* expressing mCherry for 5 min. The cells were washed and images were then taken using a fluorescence inverted microscope at ~3-s intervals for 4 min or at ~50-s intervals for 28 min. The elapsed time is indicated. Scale bar: 5 μm (A) or 1 μm (C). (B) MEFs stably expressing Atg9L1-GFP were fixed and immunostained with anti-EEA1 antibodies. Scale bar: 20 μm. (D) MEFs stably expressing Atg9L1-SECFP and EYFP-LC3 were infected with *S. typhimurium* expressing mCherry for 5 min at an MOI of 100 and images were taken as in (A) and (C) at ~30-s intervals for 10 min. Scale bar: 1 μm.

abolished EEA1 localization, which binds to endosomal membranes via PI3P (Patki *et al.*, 1997). However, the percentage of GFP-LC3–positive *S. typhimurium* was not decreased in wortmannin-treated cells (36.3 ± 6.7%) compared to control cells (25.9 ± 5.4%). Likewise, Atg5 was efficiently recruited to *S. typhimurium* in cells treated with wortmannin during *S. typhimurium* infection (Figure 5B), although the localization of Atg5 during macroautophagy was also affected by wortmannin treatment (Mizushima *et al.*, 2001). Furthermore, GFP-LC3 was efficiently and comparably recruited in Atg14L KO and Atg14L *flox/flox* MEFs (Figure 5, D and E). In sharp contrast to these findings, GFP-WIPI-1, the localization of which depends on the PI3P-binding capacity, was dispersed from *S. typhimurium* by wortmannin treatment (Figure 5C). Collectively, these data indicate that Atg5 and LC3 are recruited to *S. typhimurium* independent of the Atg9L1-PI3K axis.

Atg9L1 and FAK family-interacting protein of 200 kDa are required for the formation of the double-membrane structure surrounding *S. typhimurium*

We further pursued the nature of the LC3-positive structures in Atg9L1 KO cells by using electron microscopy (EM) to examine the LC3-positive membrane structure during *S. typhimurium* infection. GFP-LC3–expressing MEFs were infected with *S. typhimurium*, and the cells were fixed 30 min postinfection. Correlative light microscopy–electron microscopy (CLEM) revealed that *S. typhimurium* was surrounded by GFP-LC3 signals. All of the obtained images showed that *S. typhimurium* was enclosed in a single membrane structure, and additionally, a double-membrane structure surrounded the single-membrane structure (Figure 6A). In some instances, a bent single-membrane sac, which is homologous to the isolation membrane in macroautophagy, was associated instead of the double membrane (Figure 6A). These findings indicate that an autophagosome-like double membrane captured *S. typhimurium* while it was enclosed within the SCV. By contrast, GFP-LC3–positive *S. typhimurium* in Atg9L1 KO cells was surrounded only by a single membrane and lacked the double membrane or isolation membrane-like structure (Figure 6B). Furthermore, we could not observe any obvious membrane and/or vesicular structures surrounding the single membrane containing *Salmonella* (Figures 6 and S4, A and B). The same results were obtained in FAK family-interacting protein of 200 kDa (FIP200) KO cells (Figure S5B). Therefore we suggest that formation of the autophagosome-like double-membrane structure is greatly abolished in Atg9L1 and FIP200 KO MEFs. These results indicate that Atg9L1 and FIP200 are absolutely required for the formation of the double membrane. Furthermore, GFP-LC3 is recruited to *S. typhimurium*-containing vacuoles even in the absence of the Atg9L1- and FIP200-dependent double-membrane structure. We contend that LC3s are less important for membrane elongation, because the autophagosome-like membrane surrounding *Salmonella* was observed in Atg7 KO MEFs (Figure S5A) and Atg5 KO MEFs (Zheng *et al.*, 2009). During *S. typhimurium* infection, the cells were treated with Lysotracker to label the acidic compartment. After 2 h, we compared the labeling of GFP-LC3–positive *S. typhimurium*. The ratio of Lysotracker-positive *S. typhimurium*

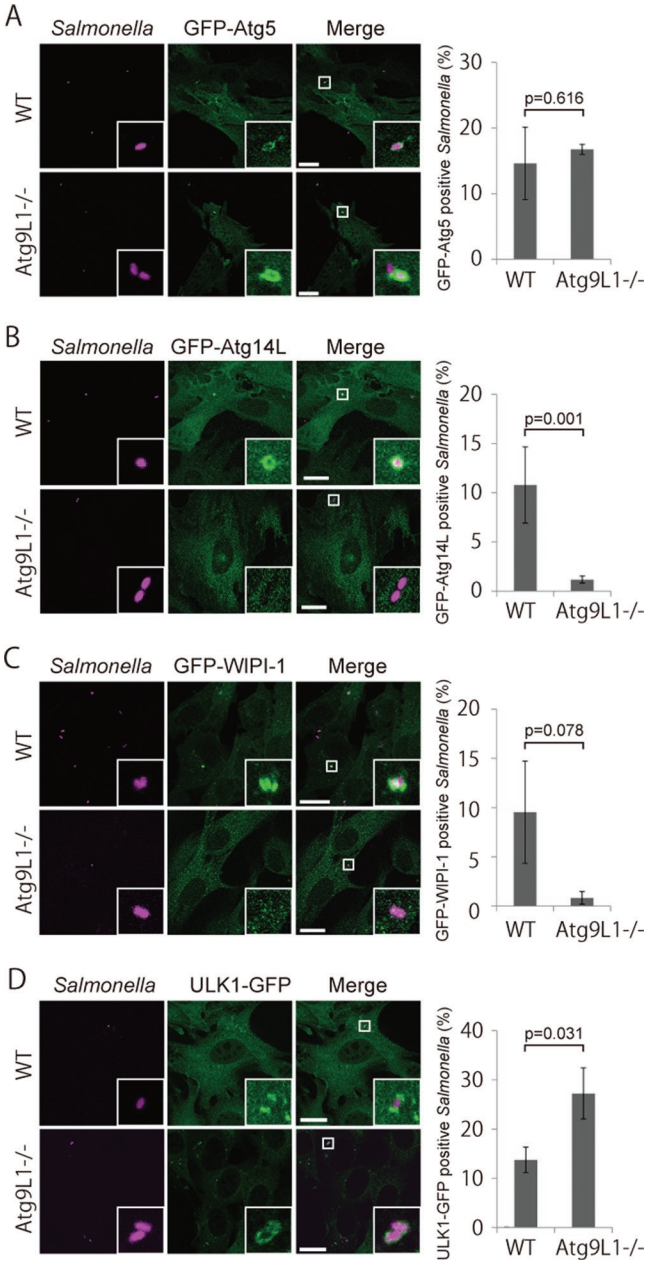

FIGURE 4: Localization of Atg proteins in Atg9L1 KO cells. Atg9L1 KO MEFs and the parental wild-type cells stably expressing GFP-Atg5 (A), GFP-Atg14L (B), GFP-WIPI-1 (C), or ULK1-GFP (D) were infected with *S. typhimurium* expressing mCherry for 1 h. After fixation, images were taken. The number of Atg-positive bacteria for each condition was determined and the percentages per all bacteria are shown. The average ± SD is shown for three independent experiments where at least 100 bacteria were counted. Scale bar: 20 μm.

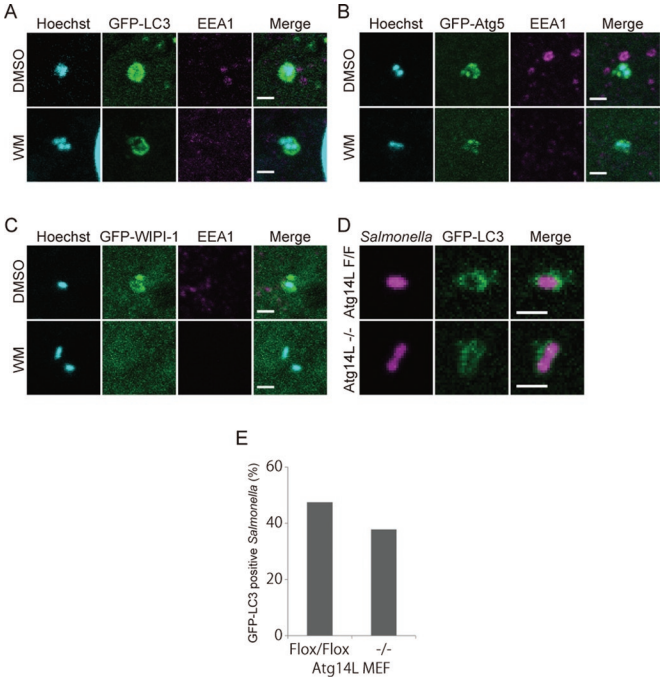

FIGURE 5: The effects of wortmannin on the association of each Atg protein with *S. typhimurium*. MEFs stably expressing GFP-LC3 (A), GFP-Atg5 (B), or GFP-WIPI-1 (C) were treated with 100 nM wortmannin for 15 min prior to infection. The cells were infected with *S. typhimurium* for 30 min at an MOI of 40, washed, fixed, and then immunostained with anti-EEA1 antibodies and stained with Hoechst 33342. Scale bar: 2 μm. (D, E) MEFs stably expressing GFP-LC3 were infected with *S. typhimurium* expressing mCherry for 1 h at an MOI of 10 and then washed. The samples were fixed, and the GFP-LC3 association rate was examined by fluorescence microscopy. At least 100 bacteria were counted. Scale bar: 2 μm.

was similar between wild-type and Atg9L1 KO cells (Figure S6, A and B). These results indicated that the maturation of the GFP-LC3–positive acidic compartment is not affected by the absence of Atg9L1.

FIP200 and Atg9L1 recycle interdependently from the proximity of *S. typhimurium*

FIP200 is a subunit of an uncoordinated 51-like kinase (ULK1) protein kinase complex consisting of FIP200, Atg101, Atg13, and ULK1 (Ganley *et al.*, 2009; Hosokawa *et al.*, 2009; Jung *et al.*, 2009). This complex is thought to be the mammalian counterpart to the yeast Atg1 protein kinase complex that is essential for autophagy (Mizushima, 2010). FIP200 KO cells have severe defects in autophagy (Hara *et al.*, 2008). We investigated the growth of *S. typhimurium* in FIP200 KO cells, and as in other Atg cells, the growth of *S. typhimurium* was not suppressed (Figure 1H). As shown in Figure 7, A, B, and G, GFP-LC3 and GFP-Atg5 were efficiently recruited to *S. typhimurium* in FIP200 KO cells, as in Atg9L1 KO cells. Similar to Atg9L1 KO cells, GFP-Atg14L and GFP-WIPI-1 localization was severely affected in FIP200 KO cells (Figure 7, C, D, and G). One potential cause for these similar localization defects in Atg9L1 KO cells and FIP200 KO cells is that Atg9L1 is not properly recruited to *S. typhimurium* in FIP200 KO cells. However, Atg9L1 was recruited to *S. typhimurium* even in FIP200 KO cells (Figure 7E). Another possibility is that the ULK1 complex is not targeted to *S. typhimurium* in Atg9L1 KO cells. However, this possibility is also not the case, as ULK1 localization to *S. typhimurium* was not affected in Atg9L1 KO cells, although it was defective in FIP200 KO cells (Figure 7F). Thus, both Atg9L1 and FIP200 are required for Atg14L-WIPI-1 to localize to *S. typhimurium*, but are not required for each other's localization. Interestingly, high levels of Atg9L1 accumulated around *S. typhimurium* in FIP200 KO cells compared to wild-type cells (Figure 7G). These findings indicate that the recycling of Atg9L1 from the proximity of *S. typhimurium* is defective in FIP200 KO cells. Likewise, ULK1 accumulated to high levels in Atg9L1 KO cells compared to wild-type cells (Figure 4D). These results suggest that Atg9L1 and the ULK1 complex

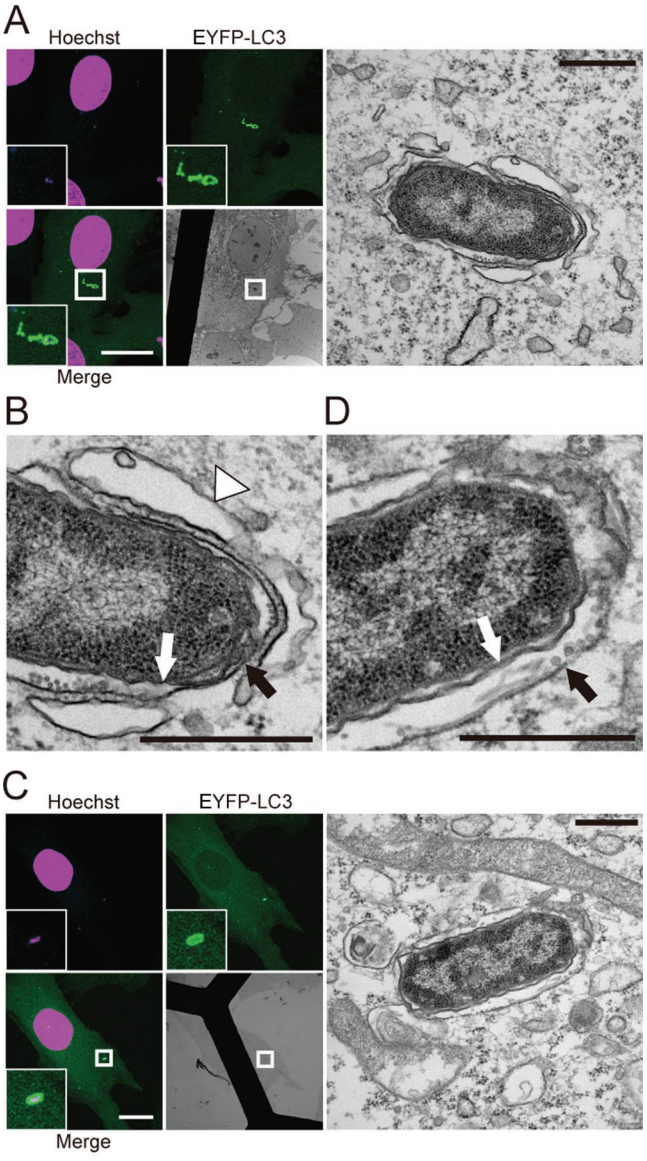

E

	single membrane	multiple membrane	
wild-type	0 (0%)	18 (100%)	n=18
Atg9L1 -/-	24 (100%)	0 (0%)	n=24

FIGURE 6: CLEM analysis of EYFP-LC3–associated membranes. Wild-type (A and B) or Atg9L1 KO MEFs (C and D) stably expressing EYFP-LC3 were cultured on gridded, glass bottom dishes and then infected with *S. typhimurium* for 30 min. The cells were fixed and stained with Hoechst 33342. GFP-LC3–positive *S. typhimurium* was observed using a confocal laser scanning microscope. The same specimens were further examined by EM. The electron micrographs were taken in the same sample field as the transmission electron microscope. White scale bar: 20 μm; black scale bar: 500 nm. (E) Quantification of the number of single or multiple membranes surrounding *S. typhimurium* in wild-type or Atg9L1 KO MEFs.

are important for each other's recycling from the area containing *S. typhimurium*.

DISCUSSION

In this study, we have identified three key points regarding *Salmonella* xenophagy: 1) An autophagosome-like double-membrane structure captures *S. typhimurium* while it is still within the SCV. 2) Atg9L1 is required to form the isolation membrane-like double-membrane structure. 3) The recruitment of LC3 to *S. typhimurium* is independent of both the Atg9L1-PI3K axis and ULK1 complex.

Our time-lapse imaging data indicate that *S. typhimurium* is already enclosed within an Atg9L1-positive membrane structure before LC3 recruitment. Significantly, both Atg9L1 and LC3 surround *S. typhimurium* for a certain time period. This finding strongly suggests that the LC3-positive double membrane surrounds an Atg9L1-positive membranous structure. Our EM images also support this model. Therefore, as suggested in a recent review (Huang and Brumell, 2009), *S. typhimurium* is enclosed in a single membrane structure, the SCV, which is surrounded by a double-membrane structure. This membrane morphology, which is surrounded by a double membrane when the bacterium escapes into the cytosol, is not similar to the xenophagy of other bacteria, such as the group A streptococcus (Yamaguchi *et al.*, 2009). In the case of *Shigella*, bacteria-induced rupture of the endosomal membrane provokes xenophagy (Paz *et al.*, 2010). *S. typhimurium* that is associated with LC3 also has been shown to associate with ubiquitin, which suggests that there is a pore that is accessible from the cytosol (Birmingham *et al.*, 2006). Thus, it is possible that SCV membrane rupture is also important for *Salmonella* xenophagy.

We showed that Atg9L1 is required to generate the isolation membrane during xenophagy. This finding is consistent with a previous observation that macroautophagosome formation is defective during macroautophagy in mammalian and yeast Atg9 mutants (Noda *et al.*, 2000; Saitoh *et al.*, 2009). Significantly, an autophagy-specific PI3K (Atg14L) and its downstream effector, WIPI-1, failed to be recruited to *S. typhimurium* in Atg9L1 KO cells (Figure 8). Atg14L/Barkor was also previously shown to be important in suppressing *S. typhimurium* growth (Sun *et al.*, 2008). Thus defects in isolation membrane generation in Atg9L1 KO cells are at least partially due to defects in the autophagy-specific PI3K. It should be noted that Atg9L1 ultimately disappeared from *S. typhimurium*, although the LC3 signals remained. This suggests that Atg9L1 cycles between the SCV and a peripheral pool that includes the Golgi and early endosomes. We showed that FIP200 is important for this recycling (Figure 7, E and G, and Figure 8). A similar recycling defect has been observed during macroautophagy in ULK1-defective cells (Young *et al.*, 2006; Hara *et al.*, 2008), and also in a yeast Atg1 mutant (Reggiori *et al.*, 2004). Furthermore, we noted that ULK1 accumulated near *S. typhimurium* in Atg9L1 KO cells, indicating that ULK1 recycling is abolished (Figures 4D and 8). Therefore Atg9L1 and the ULK1 complex are important for each other's recycling from proximity to *S. typhimurium*. We suggest that the recycling of these molecules is tightly coupled with the generation of the isolation membrane.

To our surprise, LC3 is recruited to *S. typhimurium* through a mechanism that is independent of Atg9L1, PI3K, and FIP200. Significantly, the Atg16L complex is also recruited near *S. typhimurium*. We previously showed that the localization of the Atg16L complex to any membrane is sufficient to recruit and convert LC3-I to LC3-II, and the Atg16L complex plays a key role in this process (Fujita *et al.*, 2008b). Therefore we propose that the Atg16L-E3 complex is recruited in close proximity to *Salmonella* even in the absence of Atg9L1.

Among the examined Atg proteins, only the ubiquitination-like reaction system, including Atg7, Atg3, and Atg5, is required for LC3 recruitment. These results are not consistent with a previous report

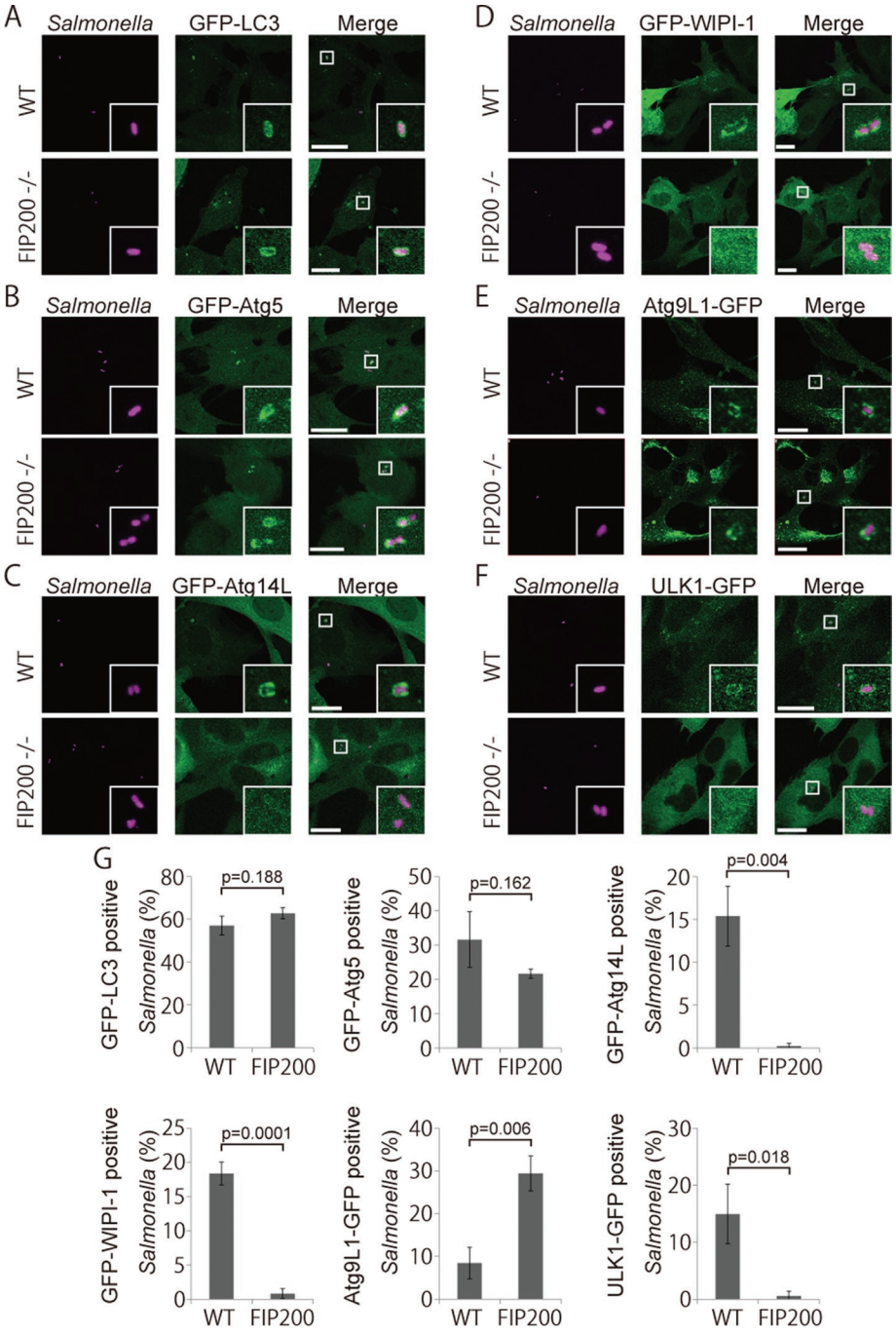

FIGURE 7: Association of Atg proteins with *S. typhimurium* in FIP200 KO MEFs. Wild-type or FIP200 KO MEFs stably expressing GFP-LC3 (A), GFP-Atg5 (B), GFP-Atg14L (C), GFP-WIPI-1 (D), Atg9L1-GFP (E), or ULK1-GFP (F) were infected with *S. typhimurium* expressing mCherry for 1 h. The cells were fixed and observed. (G) The percentage of bacteria associated with the Atg proteins was determined by fluorescence microscopy. The average ± SD is shown for at least three independent experiments where at least 100 bacteria were examined. Scale bar: 20 μm.

that LC3 recruitment to the autophagosome formation site is abolished by wortmannin treatment and in FIP200 KO cells (Hara *et al.*, 2008; Itakura and Mizushima, 2010). However, LC3 lipidation still occurred in FIP200, Atg14L, Atg9L1, and Vps34 KO cells, and LC3 was targeted to an unidentified membrane other than the autophagosome (Hara *et al.*, 2008; Matsunaga *et al.*, 2009; Saitoh *et al.*, 2009; Zhou *et al.*, 2010). Thus we would like to point out that the defect in LC3 recruitment to the autophagosome formation site in macroautophagy may be due to the lack of a native isolation membrane as the target. During *Salmonella* xenophagy in Atg9L1 KO cells, the SCV acts as an alternative target membrane and therefore can recruit LC3 (Figure 8). In wild-type cells, the isolation membrane would be the preferential target of LC3 lipidation over the SCV (Figure 8). Wortmannin is a potent inhibitor of LC3 membrane targeting and lipidation in macroautophagy. We reasoned that the unnatural target membrane of LC3 observed in Vps34 KO and Atg14L KO cells during macroautophagy may be affected because wortmannin inhibits *all* classes of PI3K. We propose that LC3 targeting depends on the presence of three factors: a target membrane, a lipidation system, and some unknown targeting mechanism, but that this targeting is independent of Atg9L1, PI3K, and ULK1. What is the targeting mechanism of the LC3-lipidation machinery? It is possible that ubiquitin and its adaptor proteins (p62/SQSTM1, NDP52) directly recruit LC3, and/or formin-binding protein 1-like (FNBP1L) directly recruits Atg3 (Huett *et al.*, 2009; Thurston *et al.*, 2009; Zheng *et al.*, 2009). However, we are certain that additional unknown mechanisms also recruit the E3 Atg16L1 complex (depicted as "X" in Figure 8).

Several studies have reported that a double-membrane autophagosome-like structure accumulates in cells with a defective LC3 system (Fujita *et al.*, 2008a; Sou *et al.*, 2008; Nishida *et al.*, 2009). Even in *Salmonella* xenophagy, a double-membrane lamellar structure surrounds *S. typhimurium* in Atg5 KO and Atg9L1 KO cells as in wild-type cells, although this structure occurs less frequently (Figure 8; Zheng *et al.*, 2009). Atg9L1 is absolutely required for the formation of the double membrane, while LC3s are less important for membrane elongation, because the autophagosome-like membrane surrounding *Salmonella* was observed in Atg7 KO MEFs (Figure S5A) and Atg5 KO MEFs (Zheng *et al.*, 2009). Importantly, these autophagosomes are potentially not completely closed, and therefore LC3 is thought to be involved in the final closure of the isolation membrane (Fujita *et al.*, 2008a; Noda *et al.*, 2009). In this paper, we propose a novel xenophagy model as follows (Figure 8). First, the isolation membrane, which ultimately becomes the xenophagosome, is formed through an Atg9L1-dependent mechanism, and potentially requires PI3K and the ULK1 complex (Figure 8). The LC3-lipidation machinery is recruited independently of these proteins, but requires an unknown targeting mechanism (Figure 8). Finally, LC3 on the isolation membrane closes the isolation membrane (Figure 8). The most important point is that the LC3 recruitment system is independent of the isolation

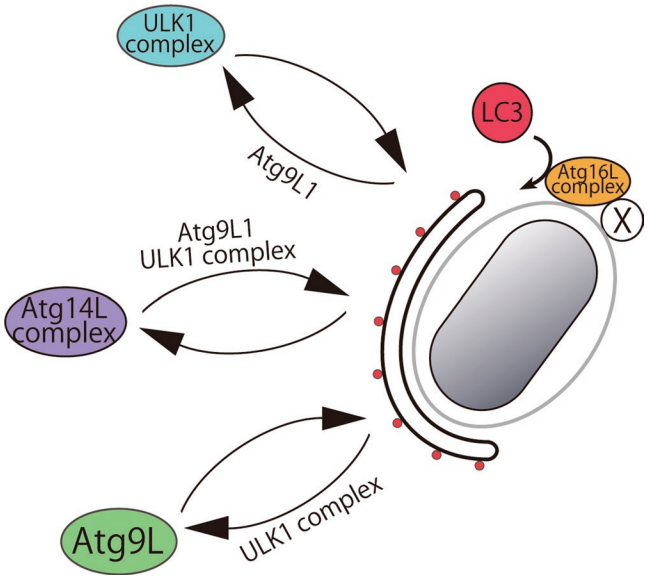

FIGURE 8: Model of Atg protein dynamics in *Salmonella* xenophagy. Atg14L, ULK1, and Atg9L1 cycle between the membrane formation site near *S. typhimurium* and another cellular pool. The cycling to and from the membrane formation site requires the indicated Atg proteins. *S. typhimurium* provides an unknown recruitment factor (X), and the Atg16L1 complex is potentially recruited near the SCV. The isolation membrane, formed independently of LC3, may be the preferable target of LC3 lipidation. In Atg9L1 KO MEFs, the isolation membrane does not form, and the SCV is the target of LC3 lipidation. Even without the LC3 system, an incomplete isolation membrane is formed.

membrane formation system. We believe this is a decent working model of autophagic processes that may also be applicable to macroautophagy and should be further examined.

MATERIALS AND METHODS

Plasmid construction and virus production

To generate pMRX-EGFP-C1-Atg5, pMRX-EGFP-C2-LC3, or pMRX-EGFP-C2-Atg14L, Atg5, LC3, or Atg14L were amplified by PCR and digested with *Kpn*I-*Not*I, *Eco*RI-*Not*I, and *Eco*RI-NotI, respectively. pEGFP-C1 and pEGFP-C2 (Clontech, Mountain View, CA) were digested with *Nhe*I, treated with Klenow fragment (Takara Bio, Shigo, Japan), and then digested with *Kpn*I and *Eco*RI, respectively. The pMRX vector was digested with *Eco*RI, treated with Klenow fragment, and then digested with *Not*I. Atg5, LC3, or Atg14L and the EGFP fragment were subcloned into the pMRX vector. To generate pMRX-ULK1-EGFP-N3 or pMRX-Atg9L1-EGFP-N1, ULK1 and Atg9L1 were PCR amplified and digested with *Eco*RI-*Bam*HI and *Eco*RI-*Sac*II, respectively. pEGFP-N3 and pEGFP-N1 were digested with *Bam*HI-*Not*I and *Sac*II-*Not*I, respectively. The PCR products and EGFP fragment were subcloned into the *Eco*RI-*Not*I sites of the pMRX vector. To generate pMRX- EYFP-C2-LC3, the EYFP sequence was PCR amplified from pEYFP-C1 (Clontech) and *Nhe*I-*Bam*HI sites were added to the N-terminus of EYFP. The products were digested with *Nhe*I-*Bgl*II and subcloned into the pEGFP-C2 vector that was digested with *Nhe*I-*Bgl*II (pEYFP-C2B). The pEYFP-C2B vector was digested with *Bam*HI-*Eco*RI. LC3 and the EYFP-C2B fragment were subcloned into the *Bam*HI-*Not*I sites of the pMRX vector. The pMRX-EGFP-WIPI-1 plasmid was a generous gift from K. Matsunaga (University of Gunma, Gunma, Japan). pMRX-IRES-puro and pMRX-IRES-bsr were kindly provided by S. Yamaoka (Tokyo Medical and Dental University, Tokyo, Japan) (Saitoh *et al.*, 2003). The pMRX-IRES-puro vector was kindly provided by T. Kitamura (University of Tokyo, Tokyo, Japan) (Morita *et al.*, 2000). Recombinant retroviruses were prepared as previously described (Saitoh *et al.*, 2003). Plat-E cells were generously provided by T. Kitamura (University of Tokyo, Tokyo, Japan) (Morita *et al.*, 2000). To generate pMRX-Atg9L1-SECFP, Atg9L1 was subcloned into the pDONR221 plasmid (Invitrogen, Carlsbad, CA) according to the manufacturer's instructions. Atg9L1-SECFP was constructed using the Multisite Gateway system (Invitrogen) (Sasaki *et al.*, 2004; Sone *et al.*, 2008). The DNA fragment containing attR1, ccdB, Cm^R, and attR2 was PCR amplified from pAd/CMV/V5-DEST (Invitrogen) and digested with *Bgl*II-*Not*I. The fragment was subcloned into the *Bam*HI-*Not*I sites of pMRX (pMRX-DEST). The pENTR-Atg9L1-SECFP sequence was transferred into the pMRX-DEST vector using an LR reaction.

Host cell culture

MEFs, NIH3T3, and Plat-E cells were cultured in DMEM D6429 (Sigma-Aldrich, St. Louis, MO) containing 10% fetal bovine serum (FBS), 4 mM L-glutamic acid, 5 U/ml penicillin, and 50 U/ml streptomycin at 37°C with 5% CO_2. Stable transformants were selected in medium containing 1 μg/ml puromycin or 10 μg/ml blasticidin. For wortmannin treatment, 1 mg/ml wortmannin (Sigma) was dissolved in dimethyl sulfoxide (DMSO) and added at a final concentration of 100 nM.

Bacterial infection

Salmonella enterica serovar Typhimurium SR-11 x3181 was used as the wild-type strain and routinely cultured in supplemented LB. *Salmonella* harboring the pBR-mCherry or pBR-mRFP plasmid, which expresses mCherry or mRFP under a constitutive promoter in pBR322 (Birmingham *et al.*, 2006), respectively, was routinely cultured in lysogeny broth (LB) supplemented with ampicillin (100 μg/ml). Bacteria were grown overnight at 37°C, and then subcultured at 1:33 for 3 h in LB without antibiotics. The bacterial inocula were prepared by pelleting at 10,000 × *g* for 2 min, and were then added to host cells at a multiplicity of infection (MOI) of 10–100 at 37°C with 5% CO_2.

Indirect immunofluorescence analysis

Samples were fixed with 4% paraformaldehyde for 10 min, quenched with 50 mM NH_4Cl/phosphate-buffered saline (PBS), permeabilized with 50 μg/ml digitonin/PBS, blocked with 0.5% bovine serum albumin (BSA)/PBS and then incubated with the indicated primary antibodies (anti-EEA1 antibodies were diluted 1:100). After washing with PBS, the samples were incubated with secondary antibodies and Hoechst 33342 (Sigma) and mounted with Slow Fade Gold (Invitrogen). Hoechst 33342/PBS was used according to the manufacturer's instructions. The samples were observed under an Olympus FV1000 confocal microscope with a 100×, 1.35 numerical aperture (NA) oil immersion objective (Olympus, Tokyo, Japan). The following antibodies were used: rabbit polyclonal anti–human EEA1 antibodies (1:100 dilution) (#2411; Cell Signaling Technology, Danvers, MA). All secondary antibodies were Alexa Fluor conjugates from Invitrogen and diluted 1:1000 in 0.5% BSA/PBS. Confocal images were imported into Adobe Photoshop and assembled in Adobe Illustrator (San Jose, CA).

Live-cell imaging

Host cells were grown in DMEM D6434 (Sigma) supplemented with 10% FBS without antibiotics on glass bottom dishes (D310300; Matsunami Glass, Osaka, Japan). After bacterial infection, the glass

bottom dish was mounted onto the microscope stage, which was equipped with a humidified environment chamber (MI-IBC, Olympus) that maintained the dish at 37°C with 5% CO_2. Images were acquired using an inverted microscope Olympus IX81 equipped with a 100×, 1.40 NA oil immersion objective (Olympus), a mercury or xenon lamp, a cooled charge-coupled device camera (Roper CoolSNAP *HQ*, Ottobrunn, Germany), and a ZDC system under the control of MetaMorph (Molecular Devices, MDS Analytical Technologies, Tokyo, Japan).

Colony formation assay

Colony formation assay was performed as previously described (Steele-Mortimer, 2008). Briefly, cells were cultured in DMEM without antibiotics and infected with *S. typhimurium* for 10 min at an MOI of 100. The cells were washed to remove extracellular *S. typhimurium* and incubated in DMEM without antibiotics for 20 min. The medium was replaced with DMEM containing 50 μg/ml gentamicin for 40 min and then replaced with medium containing 5 μg/ml gentamicin. The host cells were lysed with 1% Triton X-100 and 0.1% SDS/PBS solution, serially diluted with PBS, and spread onto LB plates.

Correlative light microscopy–electron microscopy (CLEM)

Host cells stably expressing EYFP-LC3 were cultured on glass bottom dishes with a grid pattern (P35G-2–14-C-GRID; MatTek, Ashland, MA) and infected with *S. typhimurium* for 30 min. The cells were fixed with 4% (wt/vol) formaldehyde in 30 mM HEPES buffer (pH 7.4) containing 100 mM NaCl, 2 mM $CaCl_2$, and 1 μg/ml Hoechst 33342 for 30 min at room temperature; washed in 30 mM HEPES buffer (pH 7.4) containing 100 mM NaCl and 2 mM $CaCl_2$; and examined using a confocal laser scanning microscope (FV1000; Olympus). The same specimens were further incubated with 2% (wt/vol) formaldehyde and 2.5% (wt/vol) glutaraldehyde in 30 mM HEPES buffer (pH 7.4) containing 100 mM NaCl and 2 mM $CaCl_2$ at 4°C overnight. After three washes in 30 mM HEPES buffer (pH 7.4) containing 100 mM NaCl and 2 mM $CaCl_2$, the samples were postfixed with 1% (wt/vol) osmium tetroxide in 30 mM HEPES buffer (pH 7.4) containing 0.5% (wt/vol) potassium ferrocyanide, 100 mM NaCl and 2 mM $CaCl_2$ for 1 h, washed three times in distilled water, dehydrated in ethanol, and embedded in Epon812 (TAAB Laboratories Equipment, Aldermaston, UK). Ultrathin sections (70 nm thick) were stained with saturated uranyl acetate and Reynolds lead citrate solution. The electron micrographs were taken with a JEOL JEM-1011 transmission electron microscope (JEOL, Tokyo, Japan).

Statistical analysis

Statistical analyses were performed using a two-tailed unpaired *t* test; p values < 0.05 were considered statistically significant.

ACKNOWLEDGMENTS

The authors thank K. Matsunaga (Yoshimori lab) for the gift of pMX-GFP-WIPI-1 construct; Roger Y. Tsien (University of California, San Diego, CA) for kindly providing the mCherry cDNA; A. Miyawaki (Brain Science Institute, RIKEN, Japan) for kindly providing the SECFP cDNA; S. Yamaoka for the gifts of pMRX-IRES-puro vector and pMRX-IRES-bsr vector; T. Kitamura (University of Tokyo, Japan) for the gift of Plat-E cells and pMX-IRES-puro vector; N. Mizushima for the gift of Atg5−/− MEFs; M. Komatsu for the gift of Atg3−/− and Atg7−/− MEFs; the Kitasato Institute for Life Science (Tokyo, Japan), which provided *Salmonella enterica* serovar Typhimurium (SR-11 x3181); and all of the members of the Yoshimori laboratory for helpful discussions, especially N. Fujita (Yoshimori lab) for sharing the project idea. The work described in this report was supported in part by Special Coordination Funds for Promoting Science and Technology of the Ministry of Education, Culture, Sports, Science and Technology (MEXT) of Japan, and by the Takeda Science Foundation and the Kato Memorial Bioscience Foundation.

REFERENCES

Bakowski MA, Braun V, Brumell JH (2008). Salmonella-containing vacuoles: directing traffic and nesting to grow. Traffic 9, 2022–2031.

Birmingham CL, Smith AC, Bakowski MA, Yoshimori T, Brumell JH (2006). Autophagy controls Salmonella infection in response to damage to the Salmonella-containing vacuole. J Biol Chem 281, 11374–11383.

Deretic V, Levine B (2009). Autophagy, immunity, and microbial adaptations. Cell Host Microbe 5, 527–549.

Drecktrah D, Levine-Wilkinson S, Dam T, Winfree S, Knodler LA, Schroer TA, Steele-Mortimer O (2008). Dynamic behavior of Salmonella-induced membrane tubules in epithelial cells. Traffic 9, 2117–2129.

Finlay BB, Brumell JH (2000). Salmonella interactions with host cells: in vitro to in vivo. Philos Trans R Soc Lond B Biol Sci 355, 623–631.

Fujita N, Hayashi-Nishino M, Fukumoto H, Omori H, Yamamoto A, Noda T, Yoshimori T (2008a). An Atg4B mutant hampers the lipidation of LC3 paralogues and causes defects in autophagosome closure. Mol Biol Cell 19, 4651–4659.

Fujita N, Itoh T, Omori H, Fukuda M, Noda T, Yoshimori T (2008b). The Atg16L complex specifies the site of LC3 lipidation for membrane biogenesis in autophagy. Mol Biol Cell 19, 2092–2100.

Fujita N, Saitoh T, Kageyama S, Akira S, Noda T, Yoshimori T (2009). Differential involvement of Atg16L1 in Crohn disease and canonical autophagy: analysis of the organization of the Atg16L1 complex in fibroblasts. J Biol Chem 284, 32602–32609.

Ganley IG, Lam du H, Wang J, Ding X, Chen S, Jiang X (2009). U.K. ATG13. FIP200 complex mediates mTOR signaling and is essential for autophagy. J Biol Chem 284, 12297–12305.

Hara T, Takamura A, Kishi C, Iemura S, Natsume T, Guan JL, Mizushima N (2008). FIP200, a U.K.interacting protein, is required for autophagosome formation in mammalian cells. J Cell Biol 181, 497–510.

Haraga A, Ohlson MB, Miller SI (2008). Salmonellae interplay with host cells. Nat Rev Microbiol 6, 53–66.

Hosokawa N *et al.* (2009). Nutrient-dependent mTORC1 association with the U.K.-Atg13-FIP200 complex required for autophagy. Mol Biol Cell 20, 1981–1991.

Huang J, Brumell JH (2009). Autophagy in immunity against intracellular bacteria. Curr Top Microbiol Immunol 335, 189–215.

Hueck CJ (1998). Type III protein secretion systems in bacterial pathogens of animals and plants. Microbiol Mol Biol Rev 62, 379–433.

Huett A, Ng A, Cao Z, Kuballa P, Komatsu M, Daly MJ, Podolsky DK, Xavier RJ (2009). A novel hybrid yeast-human network analysis reveals an essential role for FNBP1L in antibacterial autophagy. J Immunol 182, 4917–4930.

Ichimura Y *et al.* (2000). A ubiquitin-like system mediates protein lipidation. Nature 408, 488–492.

Itakura E, Kishi C, Inoue K, Mizushima N (2008). Beclin 1 forms two distinct phosphatidylinositol 3-kinase complexes with mammalian Atg14 and UVRAG. Mol Biol Cell 19, 5360–5372.

Itakura E, Mizushima N (2010). Characterization of autophagosome formation site by a hierarchical analysis of mammalian Atg proteins. Autophagy 6, 764–776.

Jung CH, Jun CB, Ro SH, Kim YM, Otto NM, Cao J, Kundu M, Kim DH (2009). U.K.Atg13-FIP200 complexes mediate mTOR signaling to the autophagy machinery. Mol Biol Cell 20, 1992–2003.

Kabeya Y, Mizushima N, Ueno T, Yamamoto A, Kirisako T, Noda T, Kominami E, Ohsumi Y, Yoshimori T (2000). LC3, a mammalian homologue of yeast Apg8p, is localized in autophagosome membranes after processing. EMBO J 19, 5720–5728.

Komatsu M *et al.* (2006). Loss of autophagy in the central nervous system causes neurodegeneration in mice. Nature 441, 880–884.

Kuma A, Hatano M, Matsui M, Yamamoto A, Nakaya H, Yoshimori T, Ohsumi Y, Tokuhisa T, Mizushima N (2004). The role of autophagy during the early neonatal starvation period. Nature 432, 1032–1036.

Levine B (2005). Eating oneself and uninvited guests: autophagy-related pathways in cellular defense. Cell 120, 159–162.

Matsunaga K, Morita E, Saitoh T, Akira S, Ktistakis NT, Izumi T, Noda T, Yoshimori T (2010). Autophagy requires endoplasmic reticulum

targeting of the PI3-kinase complex via Atg14L. J Cell Biol 190, 511–521.
Matsunaga K *et al*. (2009). Two Beclin 1-binding proteins, Atg14L and Rubicon, reciprocally regulate autophagy at different stages. Nat Cell Biol 11, 385–396.
Mizushima N (2010). The role of the Atg1/U.K. complex in autophagy regulation. Curr Opin Cell Biol 22, 132–139.
Mizushima N, Yamamoto A, Hatano M, Kobayashi Y, Kabeya Y, Suzuki K, Tokuhisa T, Ohsumi Y, Yoshimori T (2001). Dissection of autophagosome formation using Apg5-deficient mouse embryonic stem cells. J Cell Biol 152, 657–668.
Morita S, Kojima T, Kitamura T (2000). Plat-E: an efficient and stable system for transient packaging of retroviruses. Gene Ther 7, 1063–1066.
Nakatogawa H, Suzuki K, Kamada Y, Ohsumi Y (2009). Dynamics and diversity in autophagy mechanisms: lessons from yeast. Nat Rev Mol Cell Biol 10, 458–467.
Nishida Y, Arakawa S, Fujitani K, Yamaguchi H, Mizuta T, Kanaseki T, Komatsu M, Otsu K, Tsujimoto Y, Shimizu S (2009). Discovery of Atg5/Atg7-independent alternative macroautophagy. Nature 461, 654–658.
Noda T, Fujita N, Yoshimori T (2009). The late stages of autophagy: how does the end begin? Cell Death Differ 16, 984–990.
Noda T, Kim J, Huang WP, Baba M, Tokunaga C, Ohsumi Y, Klionsky DJ (2000). Apg9p/Cvt7p is an integral membrane protein required for transport vesicle formation in the Cvt and autophagy pathways. J Cell Biol 148, 465–480.
Noda T, Yoshimori T (2009). Molecular basis of canonical and bactericidal autophagy. Int Immunol 21, 1199–1204.
Patki V, Virbasius J, Lane WS, Toh BH, Shpetner HS, Corvera S (1997). Identification of an early endosomal protein regulated by phosphatidylinositol 3-kinase. Proc Natl Acad Sci USA 94, 7326–7330.
Paz I *et al*. (2010). Galectin-3, a marker for vacuole lysis by invasive pathogens. Cell Microbiol 12, 530–544.
Proikas-Cezanne T, Waddell S, Gaugel A, Frickey T, Lupas A, Nordheim A (2004). WIPI-1alpha (WIPI49), a member of the novel 7-bladed WIPI protein family, is aberrantly expressed in human cancer and is linked to starvation-induced autophagy. Oncogene 23, 9314–9325.
Reggiori F, Tucker KA, Stromhaug PE, Klionsky DJ (2004). The Atg1-Atg13 complex regulates Atg9 and Atg23 retrieval transport from the pre-autophagosomal structure. Dev Cell 6, 79–90.
Saitoh T *et al*. (2009). Atg9a controls dsDNA-driven dynamic translocation of STING and the innate immune response. Proc Natl Acad Sci USA 106, 20842–20846.
Saitoh T, Nakayama M, Nakano H, Yagita H, Yamamoto N, Yamaoka S (2003). TWEAK induces NF-kappaB2 p100 processing and long lasting NF-kappaB activation. J Biol Chem 278, 36005–36012.
Sasaki Y, Sone T, Yoshida S, Yahata K, Hotta J, Chesnut JD, Honda T, Imamoto F (2004). Evidence for high specificity and efficiency of multiple recombination signals in mixed DNA cloning by the Multisite Gateway system. J Biotechnol 107, 233–243.
Sone T, Yahata K, Sasaki Y, Hotta J, Kishine H, Chesnut JD, Imamoto F (2008). Multi-gene gateway clone design for expression of multiple heterologous genes in living cells: modular construction of multiple cDNA expression elements using recombinant cloning. J Biotechnol 136, 113–121.
Sou YS *et al*. (2008). The Atg8 conjugation system is indispensable for proper development of autophagic isolation membranes in mice. Mol Biol Cell 19, 4762–4775.
Steele-Mortimer O (2008). Infection of epithelial cells with Salmonella enterica. Methods Mol Biol 431, 201–211.
Sun Q, Fan W, Chen K, Ding X, Chen S, Zhong Q (2008). Identification of Barkor as a mammalian autophagy-specific factor for Beclin 1 and class III phosphatidylinositol 3-kinase. Proc Natl Acad Sci USA 105, 19211–19216.
Thurston TL, Ryzhakov G, Bloor S, von Muhlinen N, Randow F (2009). The TBK1 adaptor and autophagy receptor NDP52 restricts the proliferation of ubiquitin-coated bacteria. Nat Immunol 10, 1215–1221.
Yamada T, Carson AR, Caniggia I, Umebayashi K, Yoshimori T, Nakabayashi K, Scherer SW (2005). Endothelial nitric-oxide synthase antisense (NOS3AS) gene encodes an autophagy-related protein (APG9-like2) highly expressed in trophoblast. J Biol Chem 280, 18283–18290.
Yamaguchi H, Nakagawa I, Yamamoto A, Amano A, Noda T, Yoshimori T (2009). An initial step of GAS-containing autophagosome-like vacuoles formation requires Rab7. PLoS Pathog 5, e1000670.
Yoshimori T, Noda T (2008). Toward unraveling membrane biogenesis in mammalian autophagy. Curr Opin Cell Biol 20, 401–407.
Young AR, Chan EY, Hu XW, Kochl R, Crawshaw SG, High S, Hailey DW, Lippincott-Schwartz J, Tooze SA (2006). Starvation and U.K.-dependent cycling of mammalian Atg9 between the TGN and endosomes. J Cell Sci 119, 3888–3900.
Zheng YT, Shahnazari S, Brech A, Lamark T, Johansen T, Brumell JH (2009). The adaptor protein p62/SQSTM1 targets invading bacteria to the autophagy pathway. J Immunol 183, 5909–5916.
Zhong Y, Wang QJ, Li X, Yan Y, Backer JM, Chait BT, Heintz N, Yue Z (2009). Distinct regulation of autophagic activity by Atg14L and Rubicon associated with Beclin 1-phosphatidylinositol-3-kinase complex. Nat Cell Biol 11, 468–476.
Zhou X, Wang L, Hasegawa H, Amin P, Han BX, Kaneko S, He Y, Wang F (2010). Deletion of PIK3C3/Vps34 in sensory neurons causes rapid neurodegeneration by disrupting the endosomal but not the autophagic pathway. Proc Natl Acad Sci USA 107, 9424–9429.